Mitigating Blind Ranges via Staggered PRI and Pulse Width Optimization

Tristan J. Hardy, Jonathan W. Owen, Patrick M. McCormick, Charles A. Mohr,
David G. Felton, Shannon D. Blunt
Radar Systems Laboratory (RSL), University of Kansas

***Abstract*—A uniform pulse repetition interval (PRI) introduces blind ranges due to transmit/receive (T/R) switching, in addition to range-Doppler ambiguities. Changing the pulse repetition frequency (PRF) on a scan-to-scan basis mitigates blind ranges, but at the cost of requiring multiple scans. Alternatively, introducing staggering at the PRI level permits the avoidance of blind ranges without the need for multiple scans, while also providing an expansion of unambiguous Doppler, though doing so also requires more sophisticated receive processing to sufficiently address the increased Doppler sidelobes. It has recently been shown that PRI staggering can be optimized to flatten the extended Doppler response. In contrast, here we explore optimization to achieve a flattened energy distribution in range for the purpose of mitigating blind ranges. Diversification of pulse duration is also considered to determine its potential impact in this context.**

***Index Terms*—PRI staggering, blind ranges, pulse eclipsing, T/R switching, range ambiguity**

I. Introduction

Pulse-Doppler radar commonly transmits a repeated waveform with a fixed PRF, resulting in the well-known tradeoff between unambiguous range $R_{\mathrm{u}} = cT_{\mathrm{PRI}}/2$ and unambiguous Doppler $F_{\mathrm{u}} = \pm 1/(2T_{\mathrm{PRI}})$, where c is the speed of light and T_{PRI} is the PRI duration. Further, the ambiguity function of a uniform PRI pulse train with repeated waveforms yields a bed-of-nails structure [1]. Deviation from the bed-of-nails structure can be achieved by introducing nonrepeating waveforms [1-3] and/or applying PRI staggering [1, 4].

Here we consider the optimization of otherwise random PRI staggering as well as pulse width modulation on a per-PRI basis as a means to extend the unambiguous range interval while also ameliorating blind ranges. The means of doing so is based on the maximization of "uneclipsed energy", which is formulated in the following sections.

A detailed analysis of random PRI staggering was recently performed in [4], followed by subsequent stagger sequence optimization to extend the unambiguous Doppler response [5]. Out of that work came the observation that the co-array notion used for sparse antenna array design likewise provides a useful tool for assessing stagger sequences [6], which is leveraged in formulating the uneclipsed energy framework. While not considered here, the restricted isometry property (RIP) that is widely invoked for compressive sensing has also recently been explored as way to evaluate goodness for stagger sequences [7].

The rather straightforward reason for blind ranges is that the use of T/R switching, whereby the receiver is turned off during pulse transmission to protect sensitive components, means that the range intervals associated with those "turn off" times are not received [8]. The related effect known as "pulse eclipsing" [9] occurs when a truncated version of the reflected waveform is received due to T/R switching. As discussed in [4], PRI staggering introduces further complexity to the impact of eclipsing.

Here, the variability of the eclipsed scattered energy over range is examined, with a relationship established between the received energy over time (range delay) and the staggered PRI co-array. Specifically, random staggering mitigates blind ranges by redistributing the otherwise lost energy, though this random redistribution can be somewhat irregular over range. Consequently, optimization of staggering based on this co-array/energy relationship is also performed as a means to flatten the distribution across range. Because it naturally fits within this framework, the impact of optimizing pulse widths (or duty cycles) is likewise considered.

A consequence of staggered PRI and pulse width modulation is the need for more sophisticated radar receive processing. Put another way, while optimization can flatten ambiguities and mitigate blind ranges, doing so in turn complicates the emission structure such that standard receive processing may not perform well. Recent work on adaptive processing for this problem can be found in [10, 11] and was a key component of the DARPA Beyond Linear Processing (BLiP) program [12]. We shall treat the existence of such algorithms as a given and therefore focus solely on transmit signal design.

II. T/R Switching & Eclipsed Energy

We assume that T/R switching coincides with the rising/falling edges of the pulse and neglect the short temporal extent of these edges (i.e. treat as instantaneous) that may introduce minor model error. An illustration of PRI staggering in the context of range-extended scattering is depicted in Fig. 1, with the blanking effect of T/R switching also shown, resulting in some echoes being eclipsed. Pulse width modulation (PWM) is likewise represented via the changing pulse widths.

This work was supported by the Office of Naval Research under Contract #N00014-23-C-1053. DISTRIBUTION STATEMENT A. Approved for public release.

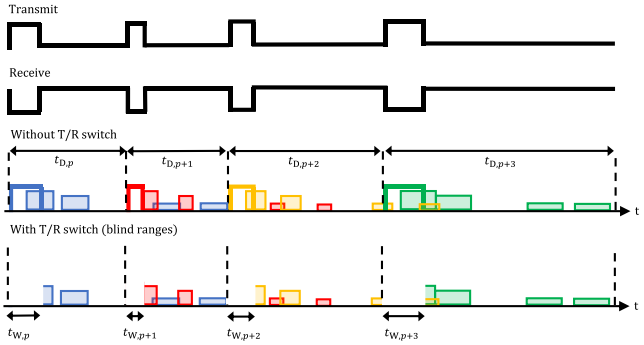

Fig. 1: T/R Diagram – Color indicates pulse number; filled squares indicate the energy envelopes of scattered reflections. Staggered PRI and PWM incur eclipsing at different ranges for each pulse, thus modifying the energy received for each range bin.

The pulse train envelope in this context is defined as

$$e(t) = \sum_{p=1}^{P} \Pi\left(\frac{t - t_{\mathrm{D},p} - \frac{t_{\mathrm{W},p}}{2}}{t_{\mathrm{W},p}}\right) = \sum_{p=1}^{P}\left(\Pi\left(\frac{t}{t_{\mathrm{W},p}}\right) * \delta\left(t - t_{\mathrm{D},p} - \frac{t_{\mathrm{W},p}}{2}\right)\right) \quad (1)$$

where $t_{\mathrm{W},p}$ indicates the pulse width and $t_{\mathrm{D},p}$ the pulse delay of the p^{th} pulse, with rectangular function $\Pi(t) = 1$ over $-0.5 < t < 0.5$ and zero otherwise. The individual PRI delays (relative to the start of the coherent processing interval (CPI)) are defined by a cumulative sum of the PRI durations $t_{\epsilon,p}$. The initial PRI duration $t_{\epsilon,1}$ is subtracted such that the cumulative delays are defined relative to time $t = 0$, such that

$$t_{\mathrm{D},p} = \left(\sum_{i=1}^{p} t_{\epsilon,i}\right) - t_{\epsilon,1} = \sum_{i=2}^{p} t_{\epsilon,i}\,. \quad (2)$$

The autocorrelation of the pulse train envelope is mathematically synonymous with the co-array (from sparse array design) [5] and accounts for the temporal extent of each rectangular pulse. For any given positive time lag, the amount of overlap between the static and shifted envelopes in the autocorrelation operation indicates the corresponding amount of eclipsed energy (that is, the energy obfuscated by a blind-range component). The co-array is therefore

$$c(\tau) = e(t) * e(-t) = \sum_{q=1}^{P}\sum_{p=1}^{P}\left(\begin{array}{c}\Pi\left(\frac{t}{t_{\mathrm{W},p}}\right) * \Pi\left(\frac{t}{t_{\mathrm{W},q}}\right) \\ * \,\delta\left(t - \left(t_{\mathrm{D},p} - t_{\mathrm{D},q} + \frac{t_{\mathrm{W},p}}{2} - \frac{t_{\mathrm{W},q}}{2}\right)\right)\end{array}\right). \quad (3)$$

The amount of uneclipsed energy may conversely be defined as the uneclipsed energy for each time lag as

$$\tilde{c}(\tau) = E_{\mathrm{s}} - c(\tau)\,, \quad (4)$$

where E_{s} is the total transmit energy in the pulse train envelope.

The relationship between the co-array $c(\tau)$ and the uneclipsed energy $\tilde{c}(\tau)$ is shown in Fig. 2 for a uniform PRI and a random PRI pulse train (no PWM), where the latter is constructed by cumulatively summing delays with a 20% uniformly-distributed deviation from the average PRI. Normalizing these by total energy E_{s} yield a percentage. The result is an energy trace representing the amount of uneclipsed energy received at each delay.

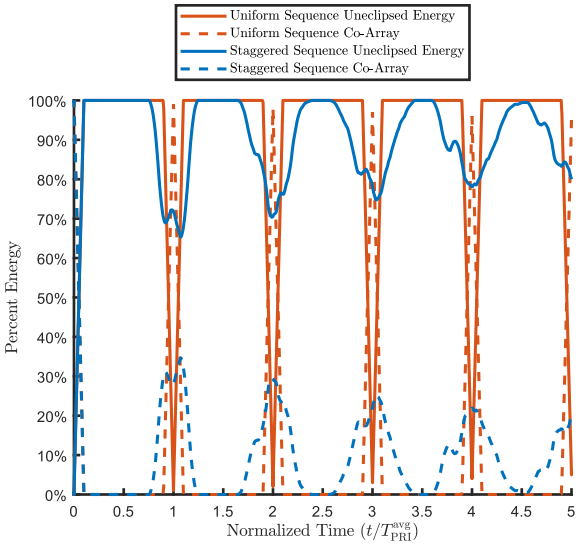

Fig. 2: Co-array $c(\tau)$ indicating eclipsed energy and the percent uneclipsed energy $\tilde{c}(\tau)$ over delay. Results are shown for a uniform PRI sequence and randomly staggered PRI sequence, with no PWM.

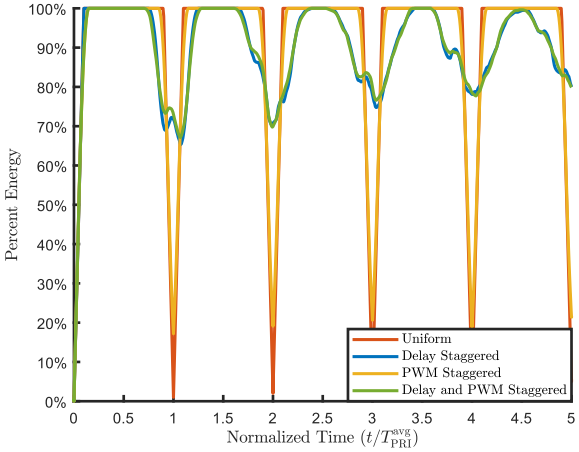

Fig. 3: Percent of uneclipsed energy $\tilde{c}(\tau)$ across delay for 1) uniform PRI with no PWM, 2) randomly staggered PRI with no PWM, 3) uniform PRI with random PWM, and 4) random staggered PRI with random PWM. Staggering dithers from the average PRI by 15%, while PWM dithers from the average pulse width by 50%.

Further examples of $\tilde{c}(\tau)$ are shown in Fig. 3, including a pulse train having 1) uniform PRI with no PWM, 2) randomly staggered PRI with no PWM, 3) uniform PRI with random PWM, and 4) randomly staggered PRI with random PWM. For case 1, the blind ranges are clearly visible at integer multiples of the fixed PRI. In contrast, case 2 introduces random staggering that significantly alleviates the impact of blind ranges, though somewhat less uneclipsed energy is obtained at some other ranges as a trade-off. For case 3, uniform PRI with random PWM only mildly alleviates pulse eclipsing effects, leaving much to be desired, which carries over into case 4 to modestly improve staggering alone. Notice that the energy distribution across delay for the random staggering cases is not flat, indicating that energy allocation at the extended range intervals is unequally distributed. Consequently, optimization of staggering and PWM bears consideration.

II. Maximizing Uneclipsed Energy

It is desirable to achieve uniform energy coverage in range to support downstream detection processing. To maximize and flatten the energy distribution over some prescribed extended range interval of $\tilde{c}(\tau)$, an equivalent problem is to minimize the co-array $c(\tau)$ over the same extended interval. Because the co-array is symmetric, minimization can be performed for the positive delay bins only. The objective function is defined in terms of the L_ϱ-norm metric

$$J = \left(\int_{\tau_1}^{\tau_2} [c(\tau)]^\varrho \, d\tau \right)^{1/\varrho} . \tag{5}$$

Components of the co-array $c(\tau)$ can be expressed as a sum of delay-shifted trapezoids that are formed by the convolution of rectangular functions $\Pi\left(\frac{t}{t_{\mathrm{W},p}}\right) * \Pi\left(\frac{t}{t_{\mathrm{W},q}}\right)$ in (3). These trapezoids will have varying widths depending on the p^{th} and q^{th} pulse widths. The delay offset $\delta\left(\tau - \left(t_{\mathrm{D},p} - t_{\mathrm{D},q} + \frac{t_{\mathrm{W},p}}{2} - \frac{t_{\mathrm{W},q}}{2}\right)\right)$ depends on the staggered PRI delays $t_{\mathrm{D},p}$ and $t_{\mathrm{D},q}$ of the interacting pulses. These trapezoids can be expressed as a superposition of time-shifted ramp functions, where $r(t) = t$ for $t \geq 0$ and zero for $t < 0$. The slope of the trapezoid edges is unitary due to the assumed constant amplitude of each pulse. Thus, the co-array in (3) simplifies to a superposition of ramp functions as

$$\begin{aligned} c(\tau) &= e(t) * e(-t) \\ &= \sum_{q=1}^{P} \sum_{p=1}^{P} \Bigg([r(\tau - t_1) - r(\tau - t_2) - r(\tau - t_3) + r(\tau - t_4)] \\ &\qquad * \delta\left(\tau - \left(t_{\mathrm{D},p} - t_{\mathrm{D},q} + \frac{t_{\mathrm{W},p}}{2} - \frac{t_{\mathrm{W},q}}{2}\right)\right) \Bigg) \end{aligned} \tag{6}$$

where

$$\begin{aligned} t_1 &= \left(-t_{\mathrm{W},p} - t_{\mathrm{W},q}\right)/2 \\ t_2 &= \left(t_{\mathrm{W},p} - t_{\mathrm{W},q}\right)/2 \\ t_3 &= \left(-t_{\mathrm{W},p} + t_{\mathrm{W},q}\right)/2 \\ t_4 &= \left(t_{\mathrm{W},p} + t_{\mathrm{W},q}\right)/2 . \end{aligned} \tag{7}$$

Because of trapezoidal symmetry, we have $t_2 = -t_3$ and $t_1 = -t_4$, making the elements in each pair interchangeable without affecting the overall outcome. The impulse delay functions in (6) can be incorporated into the ramp functions as well, permitting the simplification

$$\begin{aligned} c(\tau) &= e(t) * e(-t) \\ &= \sum_{q=1}^{P} \sum_{p=1}^{P} \left(r(\tau - \bar{t}_1) - r(\tau - \bar{t}_2) - r(\tau - \bar{t}_3) + r(\tau - \bar{t}_4) \right) \end{aligned} \tag{8}$$

with

$$\begin{aligned} \bar{t}_1 &= t_{\mathrm{D},p} - t_{\mathrm{D},q} - t_{\mathrm{W},q} \\ \bar{t}_2 &= t_{\mathrm{D},p} - t_{\mathrm{D},q} + t_{\mathrm{W},p} - t_{\mathrm{W},q} \\ \bar{t}_3 &= t_{\mathrm{D},p} - t_{\mathrm{D},q} \\ \bar{t}_4 &= t_{\mathrm{D},p} - t_{\mathrm{D},q} + t_{\mathrm{W},p} \end{aligned} \tag{9}$$

for subsequent gradient analysis. Fig. 4 provides an illustration of this sequential ramp construction of a trapezoidal function.

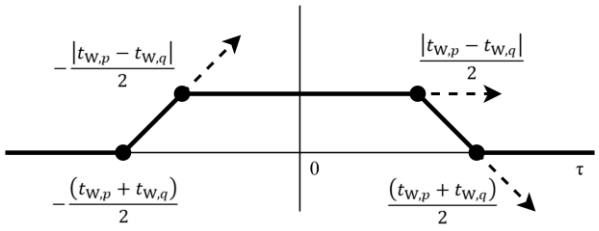

Fig. 4: Decomposition of the convolution between two pulses of inequal widths

In (8), gradients of the objective function of (5) can be determined with respect to each stagger intervals $t_{\mathrm{D},p}$ and pulse width $t_{\mathrm{W},p}$. Both gradients are derived in the Appendix. Additional constraints are imposed to bound the feasible relative staggers and pulse widths, while simultaneously enforcing constant total transmit energy E_s and a fixed CPI duration T_{CPI}. The constrained optimization problem is thus posed as

$$\begin{aligned} J &= \left(\int_{\tau_1}^{\tau_2} c(\tau)^\varrho \, d\tau \right)^{1/\varrho} \\ \text{s.t.} \quad & t_{\mathrm{W,min}} \leq t_{\mathrm{W},p} \leq t_{\mathrm{W,max}} \\ & t_{\epsilon,\mathrm{min}} \leq t_{\epsilon,p} \leq t_{\epsilon,\mathrm{max}} \\ & \left(\sum_{p=1}^{P} t_{\mathrm{W},p} \right) - E_\mathrm{s} = 0 \\ & \left(\sum_{p=1}^{P} t_{\epsilon,p} \right) - T_{\mathrm{CPI}} = 0 . \end{aligned} \tag{10}$$

Note that variants of optimization formulations or solvers could conceivably be applied to this problem. Our purpose here is to explore the impact of optimization without necessarily determining what is the best approach to do so.

III. Optimization Evaluation

A set of 100 pulse train envelopes were initialized and optimized across all delay for $P = 100$ pulses each. Here, both pulse delay and pulse width are normalized by the average PRI $T_{\mathrm{PRI}}^{\mathrm{avg}}$ such that the pulse width describes a relative duty cycle. The minimum and maximum bounds on the relative delays between pulses are $t_{\epsilon,\mathrm{min}} = 0.5T_{\mathrm{PRI}}^{\mathrm{avg}}$ and $t_{\epsilon,\mathrm{max}} = 1.5T_{\mathrm{PRI}}^{\mathrm{avg}}$ (or 50% dithering), while the pulse width duration is allowed to dither between $t_{\mathrm{W,min}} = 0.05T_{\mathrm{PRI}}^{\mathrm{avg}}$ and $t_{\mathrm{W,max}} = 0.15T_{\mathrm{PRI}}^{\mathrm{avg}}$ (or 5% dithering). The average duty cycle is therefore $0.10T_{\mathrm{PRI}}^{\mathrm{avg}}$ (or 10%). For each pulse train, all pulse delays and pulse widths were initialized from a random uniform distribution bounded between their respective lower and upper limits. Performance is evaluated for the initialized and optimized sets in terms of percent uneclipsed energy and the achieved extended Doppler response.

Three separate optimization cases are considered: 1) only the pulse delay is optimized (while pulse width is fixed), 2) only the pulse width is optimized (while pulse delay is fixed), and 3) both pulse delay and pulse width are jointly optimized. The initialized variables are drawn from a uniformly-distributed random distribution and therefore provide modest performance. Optimization of pulse width only, if pulse delay were fixed to a uniform PRI, would only minimally improve blind range

performance (per Fig. 3) and is therefore excluded from this evaluation.

A histogram of maximum eclipsed energy (across all delay) over 100 trials is shown in Fig. 5. As expected, joint optimization is marginally the best, while pulse delay (staggering) optimization alone is moderately better than PWM optimization alone. Relative to Fig. 3, where PWM is applied to a uniform PRI, the PWM in this context yields better performance because it is employed along with either a random or optimized staggered PRI. Of course, all three optimization approaches consistently produce co-arrays that outperform their initializations. As reference, the case of uniform PRI and uniform PWM (not shown in Fig. 5) corresponds to 100% since blind ranges are completely eclipsed.

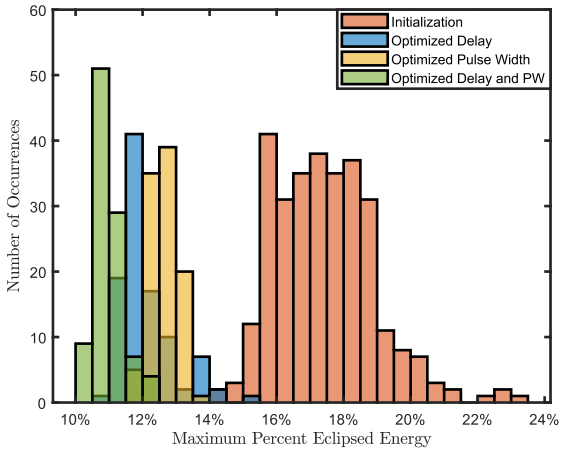

Fig. 5: Histogram of the maximum percent eclipsed energy for $P = 100$ pulses, generated from 100 Monte Carlo trials

As the number of pulses P increases, the performance distinction between the different optimization cases and from the initialization is observed to increase, while the variation in performance decreases across the trials. For instance, the average and maximum hold (worst-case) co-arrays across 100 Monte Carlo trials are shown in Fig. 6 for each optimization approach. The peak percent energy of the maximum hold co-arrays for all optimized results are significantly lower than that of the initialization, demonstrating improvements in extrema of up to 11.5%, 9.10%, and 9.96% for optimization cases 1, 2, and 3, respectively. The respective improvements in the average co-array are 5.51%, 4.53%, and 6.56% for optimization cases 1, 2, and 3, relative to the initialization. The mean and maximum hold co-array of the initialization trials demonstrates significant fluctuation, though increasing P would naturally decrease fluctuations due to the central limit theorem. The optimized co-array curves are flatter than the initialization across delay, especially when examining the maximum hold values. Clearly, optimization can improve upon a random initialization in all cases to maximize the uneclipsed energy across range. Further, the achieved plateau occurs near the average duty cycle $0.10T_{\mathrm{PRI}}^{\mathrm{avg}}$, as this is the minimum achievable eclipsed energy in the nearest range intervals. Roll-off at larger delays is due to reduction of pulse interactions.

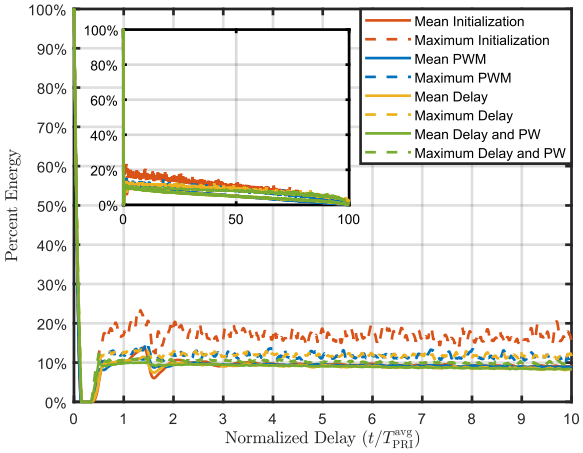

Fig. 6: Plot of the average and maximum co-array for $P = 100$ pulses, from 100 Monte Carlo trials

Next, the extended Doppler response is analyzed over the set of staggered pulse trains. This response is dependent on the delay intervals $t_{\mathrm{D},p}$, but not necessarily on the PWM values $t_{\mathrm{W},p}$. The extended Doppler response describes the expected response from a stationary scatterer, evaluating the zero-range cut. The mean and maximum Doppler beampattern of each optimization Monte Carlo are shown in Fig. 7.

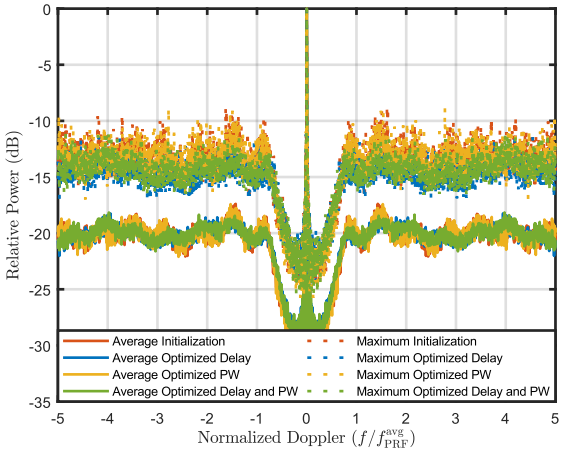

Fig. 7: Plot of average and maximum extended Doppler response for $P = 100$, from 100 Monte Carlo trials

While modest deviations occur in the Doppler response, the mean and maximum performance traces are quite similar for all cases. The observed ringing for higher normalized Doppler is the same as noted in [4]. Optimization of PWM alone has little/no effect on the Doppler response, relative to the initialization, considering that the staggers are the primary factor in this context. The distribution of the relative pulse delays for all cases is shown in Fig. 8. The optimized delay cases in blue and green both tend toward bimodal solutions, while the initialization and pulse width optimization distributions in red and yellow are uniform.

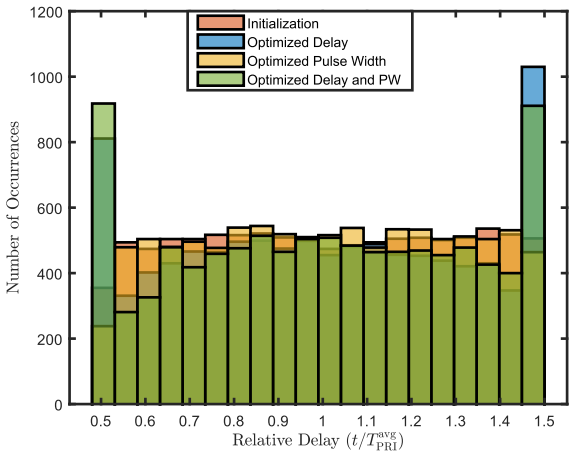

Fig. 8: Histogram of the relative pulse delays for $P = 100$, from 100 Monte Carlo trials

Further comparison can be made with the distribution of pulse widths shown in Fig. 9. For both approaches involving PWM, the green and yellow bars are also nearly bimodal. Otherwise, the methods for blue and red remain flat like the drawn uniform distribution. Optimization of both relative delay and pulse width favor bimodal distributions for their respective parameters. As such, the combined optimization produces results that favor sets of parameters near the lower and upper bound constraints, which can be viewed as maximizing the amount achievable change given the permitted bounds.

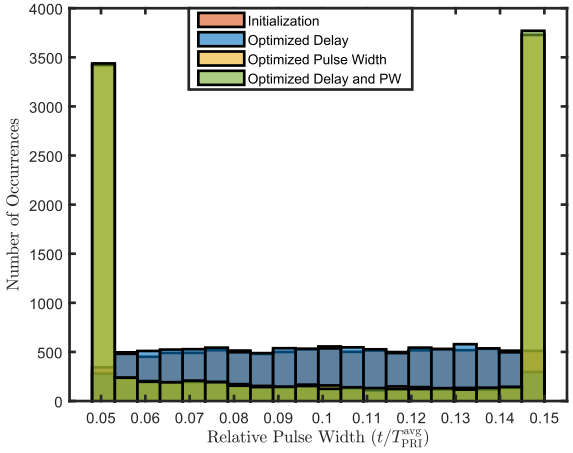

Fig. 9: Histogram of the relative pulse widths for $P = 100$, from 100 Monte Carlo trials.

VI. Conclusions

Random PRI staggering can be used to extend unambiguous range and avoid blind ranges, though the energy distribution can be somewhat irregular. Using a form of gradient descent, it has been shown that staggered pulse sequences and PWM can be optimized to maximize the uneclipsed energy across a prescribed range interval, thereby flattening the energy distribution over range. Further, while such an approach does not directly address the desire for a flattening of the extended unambiguous Doppler, results indicate that this outcome is effectively attained as a bonus. This work examines the art of the possible for this problem, with exploration using other optimization approaches encouraged.

IV. References

[1] Nadav Levanon, Eli Mozeson, “Radar Signals”, IEEE, 2004.

[2] S. D. Blunt *et al.*, "Principles and Applications of Random FM Radar Waveform Design," in *IEEE Aerospace and Electronic Systems Magazine*, vol. 35, no. 10, pp. 20-28, 1 Oct. 2020.

[3] J. Quirk, P. McCormick, J. Owen, S. Blunt, “Experimental Demo of Range Disambiguation via Slow-time Coding & Reiterative Super-Resolution”, 2024 IEEE Int’l Radar Conference, Rennes, France.

[4] S. D. Blunt, L. A. Harnett, B. Ravenscroft, R. J. Chang, C. T. Allen and P. M. McCormick, "Implications of Diversified Doppler for Random PRI Radar," in *IEEE Transactions on Aerospace and Electronic Systems*, vol. 59, no. 4, pp. 3811-3834, Aug. 2023.

[5] R. J. Chang, C. C. Jones, J. W. Owen and S. D. Blunt, "Gradient-Based Optimization of Pseudo-Random PRI Staggering," in *IEEE Transactions on Radar Systems*, vol. 1, pp. 249-263, 2023.

[6] R. J. Chang, D. B. Herr, J. W. Owen, P. M. McCormick, S. D. Blunt and J. M. Stiles, "On the Relationship Between PRI Staggering and Sparse Arrays," *2023 IEEE Radar Conference*, San Antonio, TX, USA, 2023.

[7] C. Schone, N. A. Goodman, "Use of the Restricted Isometry Property for Assessing PRI Staggering Sequences," *2024 IEEE Radar Conference*, Denver, CO, USA, 2024

[8] M. Oppermann, R. Rieger, "Multifunctional MMICs – Key Enabler for Future AESA Panel Arrays," *IMAPS Nordic Conference on Microelectronics Packaging*, Oulu, Finland, 2018, pp. 77-80.

[9] E.R. Billam, “Eclipsing effects with high-duty-factor waveforms in long-range radar,” *IEE Proc. F – Communications, Radar & Signal Processing*, vol. 132, no. 7, pp. 598-603, Dec. 1985.

[10] L. A. Harnett, B. Ravenscroft, S. D. Blunt and C. T. Allen, "Experimental Evaluation of Adaptive Doppler Estimation for PRI-Staggered Radar," *2022 IEEE Radar Conference*, New York City, NY, USA, 2022.

[11] P. Cox, K. Klein, M. Coutiño, L. Anitori, “Improved detection of hypersonic threats with radar using irregular waveforms and advanced processing,” European Defence Agency, Report, 2023.

[12] M. Yeary, D. Schvartzman, M. Herndon, R. D. Palmer, B. Epstein and F. Robey, "Fully Digital Horus Radar Experiments in Support of DARPA's Beyond Linear Processing Program," *2024 IEEE Int’l Symposium on Phased Array Systems and Technology*, Boston, MA, USA, 2024.

[13] K.B. Petersen, M.S. Pedersen, The Matrix Cookbook, Nov. 2012.

V. Appendix

The gradient chain rule is applied, first determining the partial derivative $\frac{\partial J}{\partial \lambda}$ where λ is either $t_{\mathrm{D},\bar{p}}$ or $t_{\mathrm{W},\bar{p}}$, yielding

$$\frac{\partial J}{\partial \lambda} = (J^{1-\varrho}) \cdot \int_{\tau_1}^{\tau_2} c(\tau)^{\varrho-1} \left(\frac{\partial c(\tau)}{\partial \lambda} \right) d\tau \,, \tag{11}$$

where $\bar{p} = 1, 2, \cdots, P$ indicates the pulse parameter under consideration. The derivative of the ramp function $r(t)$ is the unit step function $u(t) = 1$ for $t \geq 0$ and zero for $t < 0$. Partial derivatives are calculated under four conditions existing within the double summation, specifically $(\bar{p} = p;\ \bar{p} = q)$, $(\bar{p} = p;\ \bar{p} \neq q)$, $(\bar{p} \neq p;\ \bar{p} = q)$ and $(\bar{p} \neq p;\ \bar{p} \neq q)$. The resulting gradient with respect to stagger interval is

$$\frac{\partial c(\tau)}{\partial t_{\mathrm{D},\bar{p}}}=\sum_{q=1}^{P}\sum_{p=1}^{P}\frac{\partial}{\partial t_{\mathrm{D},\bar{p}}}\left(r(\tau-\bar{t}_1)-r(\tau-\bar{t}_2)-r(\tau-\bar{t}_3)+r(\tau-\bar{t}_4)\right)=\begin{pmatrix}\sum\limits_{\substack{\bar{q}=1\\ \bar{q}\neq p\\ \bar{q}=q}}^{P}\left(-u(\tau-\bar{t}_1)+u(\tau-\bar{t}_2)+u(\tau-\bar{t}_3)-u(\tau-\bar{t}_4)\right)\\ +\sum\limits_{\substack{\bar{p}=1\\ \bar{p}=p\\ \bar{p}\neq q}}^{P}\left(u(\tau-\bar{t}_1)-u(\tau-\bar{t}_2)-u(\tau-\bar{t}_3)+u(\tau-\bar{t}_4)\right)\end{pmatrix}. \tag{12}$$

The gradient with respect to pulse width

$$\frac{\partial c(\tau)}{\partial t_{\mathrm{W};\bar{p}}}=\begin{pmatrix}\sum\limits_{\substack{\bar{q}=1\\ \bar{q}\neq p\\ \bar{p}=q}}^{P}\left(u(t-\bar{t}_2)-u(t-\bar{t}_4)\right)+\sum\limits_{\substack{\bar{p}=1\\ \bar{p}=p\\ \bar{p}\neq q}}^{P}\left(u(t-\bar{t}_1)-u(t-\bar{t}_2)\right)\\ +\sum\limits_{\substack{p=1\\ \bar{p}=p\\ \bar{p}=q}}^{P}u\left(t-\left(-t_{\mathrm{W},p}\right)\right)-u\left(t-\left(t_{\mathrm{W},p}\right)\right)\end{pmatrix} \tag{13}$$

yields a slightly different solution because $\bar{t}_1,\bar{t}_2,\bar{t}_3,\bar{t}_4$ each have different relations to $t_{\mathrm{W},\bar{p}}$. The latter term in (13) describes the co-array mainlobe. To minimize the co-array mainlobe, the obvious solution is to uniformly minimize all pulse widths to the smallest value. Generally, the minimization bounds will not include the co-array mainlobe width and the latter term may be disregarded.

Lastly, the derivative $\frac{\partial J}{\partial t_{\epsilon,\bar{p}}}$ is determined. The chain rule in the Jacobian form [13] dictates that

$$\frac{\partial J}{\partial t_{\epsilon,\bar{p}}}=\sum_{\bar{q}=1}^{P}\frac{\partial J}{\partial t_{\mathrm{D},\bar{q}}}\frac{\partial t_{\mathrm{D},\bar{q}}}{\partial t_{\epsilon,\bar{p}}}. \tag{14}$$

Apply (11) and (12) to define $\frac{\partial J}{\partial t_{\mathrm{D},\bar{q}}}$, then $\frac{\partial t_{\mathrm{D},\bar{q}}}{\partial t_{\epsilon,\bar{p}}}$ is determined as

$$\frac{\partial J}{\partial t_{\epsilon,\bar{p}}}=\sum_{\bar{q}=1}^{P}\frac{\partial J}{\partial t_{\mathrm{D},\bar{q}}}\frac{\partial t_{\mathrm{D},\bar{q}}}{\partial t_{\epsilon,\bar{p}}}=\sum_{\bar{q}=1}^{P}\frac{\partial J}{\partial t_{\mathrm{D},\bar{q}}}\left[\frac{\partial\left(\sum_{i=2}^{\bar{q}}t_{\epsilon,i}\right)}{\partial t_{\epsilon,\bar{p}}}\right]=\sum_{\bar{q}=\bar{p}}^{P}\frac{\partial J}{\partial t_{\mathrm{D},\bar{q}}}$$
$$\frac{\partial\left(\sum_{i=2}^{\bar{q}}t_{\epsilon,i}\right)}{\partial t_{\epsilon,\bar{p}}}=\begin{cases}1 & \bar{q}>1,\bar{q}\geq\bar{p}\\ 0 & \bar{q}=1,\bar{q}\leq\bar{p}\end{cases}. \tag{15}$$

Combining terms from (11)-(15) provides the complete gradients as

$$\frac{\partial J}{\partial t_{\epsilon,\bar{p}}}=\begin{cases}\left(J^{1-\varrho}\right)\cdot\sum\limits_{\bar{q}=\bar{p}}^{P}\int_{\tau_1}^{\tau_2}c(\tau)^{\varrho-1}\begin{pmatrix}\sum\limits_{\substack{\bar{q}=1\\ \bar{q}\neq p\\ \bar{q}=q}}^{P}\left(-u(\tau-\bar{t}_1)+u(\tau-\bar{t}_2)+u(\tau-\bar{t}_3)-u(\tau-\bar{t}_4)\right)\\ +\sum\limits_{\substack{p=1\\ \bar{q}=p\\ \bar{q}\neq q}}^{P}\left(u(\tau-\bar{t}_1)-u(\tau-\bar{t}_2)-u(\tau-\bar{t}_3)+u(\tau-\bar{t}_4)\right)\end{pmatrix}d\tau & \text{for } \bar{p}=2,3,\cdots,P\\ 0 & \text{for } \bar{p}=1\end{cases} \tag{16}$$

$$\frac{\partial J}{\partial t_{\mathrm{W};\bar{p}}}=\left(J^{1-\varrho}\right)\cdot\int_{\tau_1}^{\tau_2}c(\tau)^{\varrho-1}\begin{pmatrix}\sum\limits_{\substack{\bar{q}=1\\ \bar{q}\neq p\\ \bar{p}=q}}^{P}\left(u(t-\bar{t}_2)-u(t-\bar{t}_4)\right)+\sum\limits_{\substack{\bar{p}=1\\ \bar{p}=p\\ \bar{p}\neq q}}^{P}\left(u(t-\bar{t}_1)-u(t-\bar{t}_2)\right)\\ +\sum\limits_{\substack{p=1\\ \bar{p}=p\\ \bar{p}=q}}^{P}u\left(t-\left(-t_{\mathrm{W},p}\right)\right)-u\left(t-\left(t_{\mathrm{W},p}\right)\right)\end{pmatrix}d\tau. \tag{17}$$